THE ANNALS OF "DUNAREA DE JOS" UNIVERSITY OF GALATI
FASCICLE XI – SHIPBUILDING. ISSN 1221-4620
2017

NUMERICAL SIMULATION OF A CAVITATING PROPELLER WORKING IN OPEN WATER

Adrian Lungu

"Dunarea de Jos" University of Galati
Faculty of Naval Architecture
Domneasca Street, No. 47, RO-800008, Romania
E-mail:adrian.lungu@ugal.ro

ABSTRACT

A viscous open water flow investigation around a four blade propeller model which equips the ONRT tumblehome is described in the present paper. The main purpose of the present study is that of establishing an appropriate method for computing the flow solution around a propeller working under the imminence of cavitation occurrence. The ISIS-CFD solver of FINE^{TM}/Marine software package is used to fulfill the task. The Reynolds-averaged Navier-Stokes equations in which the turbulence is modeled with the EASM model are numerically solved by using a finite-volume based method. The performance diagrams of the propeller are computed for a range of advance coefficient between 0 and 1. Comparisons with the experimental data are provided to validate the numerical approach. A detailed analysis of the flow field structure as well as of the vortical character of the flow behind the propeller is provided. A special attention will be paid to the cavitation regime for which a particular model will be proposed.

Keywords: Numerical simulation**,** ONRT tumblehome, RANSE, turbulence, vortical flow, cavitation

1. INTRODUCTION

Predictions of ship self-propulsion, maneuvering and course keeping, either in calm water or waves, are one of the most demanding challenges in ship hydrodynamics. Much attention has been paid so far not only for the accurate computation of the propeller performances, but also on the cavitation occurrence and development in time and space. This is one important issue since it has an overwhelming influence on the overall propeller performances. The viscous RANS approach has been used for the flow simulation around propeller widely since 1990s, the early works of cavitation simulation mostly targeted hydrofoils and underwater vehicles being accomplished mainly by most of the existing commercial CFD solvers. Simulating the flow around an open water propeller has as primary objective the computation of the thrust and torque and subsequently the efficiency in various working condition. The task in itself is of a great importance since may help in establishing the propeller performance diagrams needed by the self-propulsion investigation.

Cavitation generally occurs when the local pressure drops below its vapor pressure. Cavitation presents complex unsteady, turbulent and multi-phase flow phenomena with a large density difference and mass transfer. These features result in a unique challenge for the simulation of cavitating flows. Using computational models for cavitation has been around for the last few decades. Early works

© *Galati University Press, 2017*

mainly used potential flow theory. Complex characteristics of cavitating flows such as sharp changes in the fluid density, existence of a moving boundary and the requirement of modeling phase change prevented the development of computational algorithms based on the RANS equations. Following the advancement in CFD methods, cavitation models emerged in early 1990's. Among these models, the two main categories are interface tracking method and homogeneous equilibrium flow. In the first category, a constant pressure (vapor pressure) is assumed for the cavity region (the so-called cavity) and a wake model is used to predict the shape of the cavity in adaptive grids. The current study is based on the second category where a single-fluid modeling approach is employed for both phases. Homogeneous equilibrium flow model assumes that there is no velocity slip between the phases at the cavity interface. Various models in this category differ in the relation that defines the variable density field. In one model, barotropic water-vapor state laws are used to calculate density. A more precise approach is to solve an advection equation for liquid (or vapor) volume fraction and compute density according to volume fraction of the two phases.

The present paper represents a first attempt in assessing the hydrodynamic features of the free-surface flow around a ship hull equipped with significant appendages and propeller running in waves. Since an important prerequisite for any self-propulsion computation is the open water test, the work reported in here will refer only at this task. The hull chosen in the present study is the Office of Naval Research tumblehome model 5613 (ONRT hereafter), which is a preliminary design of a modern surface combatant, accessible for fundamental research purposes to the world-wide community with interests for the subject.

The geometry has been provided at the 2015 Workshop on CFD in Ship Hydrodynamics organized in Tokyo by the Japanese National Maritime Research Institute [1]. Extensive experiments were performed in IIHR [2] for the ship model and the experimental data is freely available for the community. Indeed, the great deal of existing experimental data [1], [2] represents the main reason for choosing in the present study the ONRT model since it may set the pace for performing all the numerical tests for a consistent verification and validation of the proposed theoretical study.

Aside of that, the chosen hull raises additional difficulties especially in discretizing the computational domain since comprises a generous sonar in the fore region, well-extended roll stabilizers, two significant shafts of a variable geometry, two pairs of brackets, two suspended rudders and two four-blades propellers that rotate inward, as Fig.1 shows. The main particulars of the ship are tabulated in Table 1.

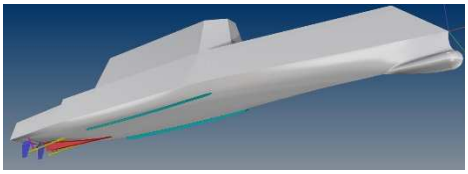

Fig. 1. ONRT hull form

Table1. Main particulars of the ONRT hull at model and full scales

Main particulars		Model scale 1/49	Full scale
Length at WL	L_{WL} [m]	3.147	154.0
Maximum beam	B_{WL} [m]	0.384	18.78
Draft	D [m]	0.266	14.50
Depth	H [m]	0.112	5.494
Displacement	Δ [kg]	72.6	$8.6 \cdot 10^6$

The four blade propeller shown in Fig.2, whose geometric particulars are tabulated in Table 2 is subjected of the following numerical study. Although the propeller diameter

© Galati University Press, 2017

for the self-propulsion investigation is 0.1066 m, for the open water numerical simulation the considered diameter is 0.25 m for reasons related only to the limitation of the scale effects. The blade geometry is almost symmetric while the hub is almost cylindrical since the propeller is a part of a twin system that works at the aft of the ship considered in the present study.

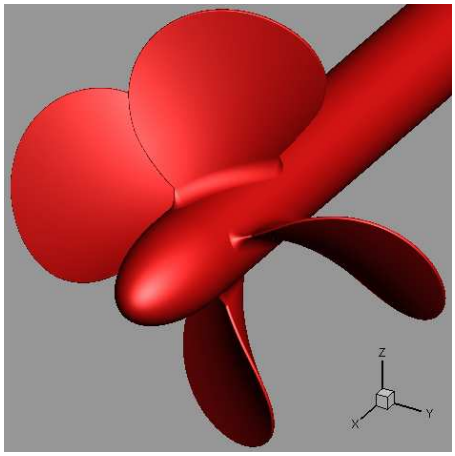

Fig. 2. ONRT propeller

Table2. Main particulars of the ONRT propeller model

Main particulars		Model scale 1/49
Propeller diameter	D_P [m]	0.1066
Propeller center, long. location (from the FP)	x/L_{WL}	0.9267
Propeller center, lateral location (from CL)	$\pm y/L_{WL}$	0.02661
Propeller center, vertical location (below the WL)	$-z/L_{WL}$	0.03565
Propeller shaft angle (downward positive)	5	5
Propeller rotation direction (view from stern)	inward	inward

2. NUMERICAL APPROACH

The ISIS-CFD flow solver is used to investigate the flow field structure around the propeller, based on a VOF approach. The solver uses algorithms providing a strong pressure-velocity coupling for the RANS equations. The simulation is accomplished in a global approach in which the momentum and mass conservation equations written in respect to a Cartesian system of coordinates are solved. Since no coordinate transformation is done in the solving algorithm, the efficiency of the numerical approach may be considered as being suited to the purpose. Dependent variables of the set of equations are the velocity and pressure. Closure to the turbulence is achieved through the EASM model of Rumsey and Gatski [3]. The integration of the forces is performed on the solid-surface cell based on the quaternions formulation. Integration in time is done in an Euler explicit way, whereas an upwind discretization scheme is used for the convective terms with a second order for the acceleration. Conservation applies to the mass and momentum and a Piccard model applies for the linearization. The pressure-correction is imposed and the Krylov technique is used for the iteration of the solution. A non-structured grid is used for the discretization of the computational domain, therefore hexahedral elements are used for that purpose. A fully unsteady approach is used to advance the solution in time.

The numerical modeling of cavitation is based on the resolution of a transport equation in which source terms are added to model the vaporization and condensation of the phases liquid/vapor. The Sauer, Merkle and Kunz models are implemented in the ISIS-CFD solver. In the Sauer model the nuclei density has to be provided as an input data therefore it has been simply neglected since the accuracy of the choice of the inputs are, up to a significant extent, subjected to a fortunate choice rather than to a rigorous one. Under such circumstances, the author had only to choose between the remaining Merk-

© *Galati University Press, 2017*

le and Kunz models for which the input data are liquid product coefficient, liquid destination coefficient and cavitation reference length. Because not only to its versatility but also to its numerical robustness the Kunz model was the choice.

The initial conditions refer to the incoming flow velocity, pressure and turbulent viscosity only. The computational domain is limited at -2.5D_P at the upstream where the velocity components and the turbulent viscosity are imposed, whereas a Neumann condition is imposed for pressure. Same boundary conditions are imposed for the lateral frontier. At the downstream, which is located at 4D_P, the velocity components and the turbulent viscosity are zero-extrapolated, whereas the pressure is frozen at the static value. The flow starts from rest and it is accelerated within 6 seconds up to the given rotational velocity.

2.1 GRID GENERATION

Whenever a viscous flow is numerically computed a sufficient number of grid points inside the boundary layer is required. A local Reynolds number based on the wall variable y^+ is computed prior to the grid generation, to estimate an appropriate cell size y_{wall} for the RANS solution. In the present study the mesh is generated by using the Hexpress module of the FINE^{TM}/Marine in which automatic refinement based on defined sensors either next to solid walls or inside specified area in the domain is possible. Fig.3 shows the computed mesh: (a) for the aft part of the ship hull as well as for the propeller considered for the open water simulation (b).

Special attention to the quality criteria such as orthogonality, smoothness and clustering is paid during the mesh generation process. Several restrictions concerning the cell clustering are imposed around all the appendages as well as inside all the intersections of different surfaces, as Fig. 3(a) clearly bears out. Similarly for the propeller, the clustering requirement is imposed around the root and tip of the blade where the gradients of the hydrodynamic variables are expected to have significantly high values, as Figs. 3(c) and 3(d) bear out.

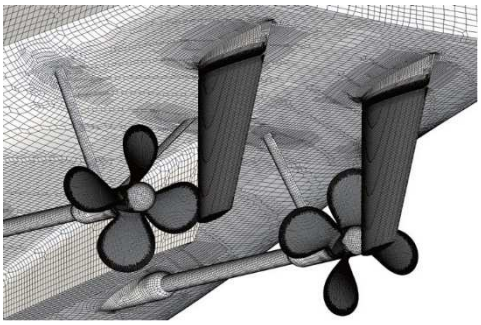

(a)

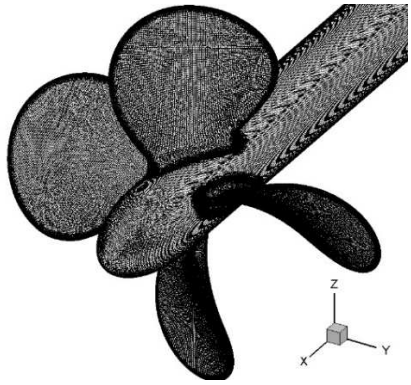

(b)

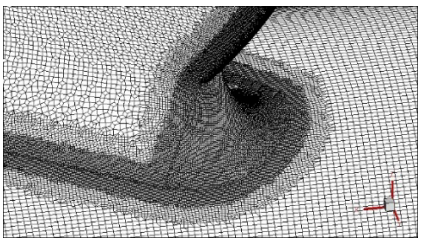

(c)

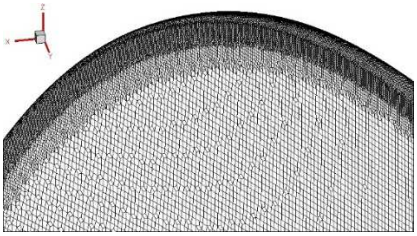

(d)

Fig. 3. Computational mesh

© Galati University Press, 2017

3. RESULTS AND DISCUSSIONS

All the computations are carried out for a rotational velocity of 1500 r.p.m. for which the inflow velocity is successively modified from zero to 10.625 m/s, so that the advance coefficient value be in between 0 and 1.7 for which the experimental data are available. The solution was computed for 10 seconds on an HPC over 120 cores, so that the propeller could perform 250 complete revolutions. For the stability reasons, the flow is accelerated from the still state to the oncoming velocity based on a half sinusoidal low over 6 seconds. The time step for advancing the solution in time is chosen at a value of $5e^{-5}$ seconds so that the Courant number remained less than unity throughout the whole computation. All the computations were performed on the same computational grid.

Figure 1 depicts a comparison between the computed open water diagrams and the corresponding experimental ones. Computed data are drawn with solid lines, while the experimental data are marked with symbols. The resemblance between the two sets of data may be considered as satisfactory since the error does not exceed 3%. Analyzing the figure, one may see that for lower advance coefficient the computed solution slightly over estimates both the K_T and K_Q. In author's opinion this is due to the mesh resolution that could not be refined more because of the limitations imposed by the computational costs in terms of the CPU time.

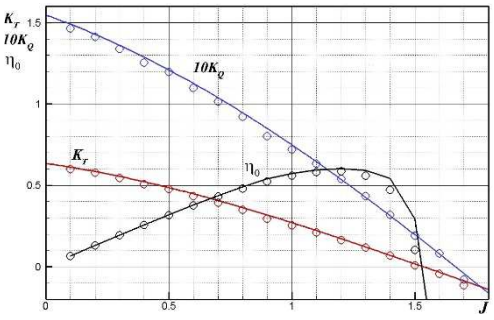

Fig. 4. Comparison between the open water diagrams computed at T=10 and measured [1]

Next, Fig. 5 proposes a comparison between the average pressure distributions on both faces of the propeller, namely on the pressure side in Fig. 5(a) and on the suction side in Fig. 5(b). Worth mentioning that the pressure is the total one, therefore it includes the static component, a fact which explains the areas of high pressure on the areas around the tip of the blades situated at 12 and 3 o'clock. Similarly, on the suction side, the negative pressure in the root areas is fairly less prominent if the same blades are considered. This finding is according to the physics of the flow phenomenon and proves that the numerical simulation produces reliable solutions. Fig. 5(b) reveals areas of negative pressure which are originating from the tips and extend downward to the blade root along with the leading edges. Since those areas are susceptible to the cavitation occurrence, more attention will be paid to them in the followings.

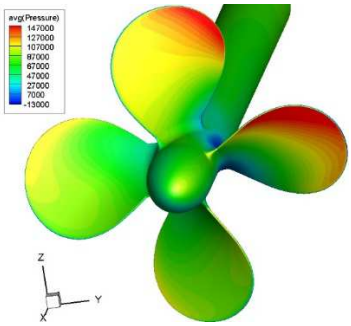

(a)

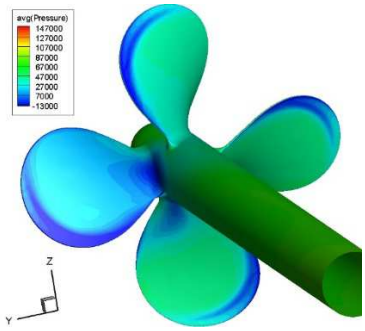

(b)

Fig. 5. Average pressure distribution on the propeller: (a)-pressure side (b)-suction side

© *Galati University Press, 2017*

Fig. 6 depicts the pressure (normal stress) distributions computed in the propeller plane and at 0.1 D_P downstream of it. The wake behind the propeller is a region that consists of complex hydrodynamic phenomena characterized by temporally and spatially fast-varying flow parameters like local fluid velocity, pressure, turbulent kinetic energy and dissipation and so on. The work done by the propeller torque is equal to the thrust in opposing the drag along with the kinetic energy of the water gained as it passes through the propeller. As a result, the flow in the propeller plane is described by strong pressure gradients, which decay rapidly in the stream as a result of the viscous dissipation.

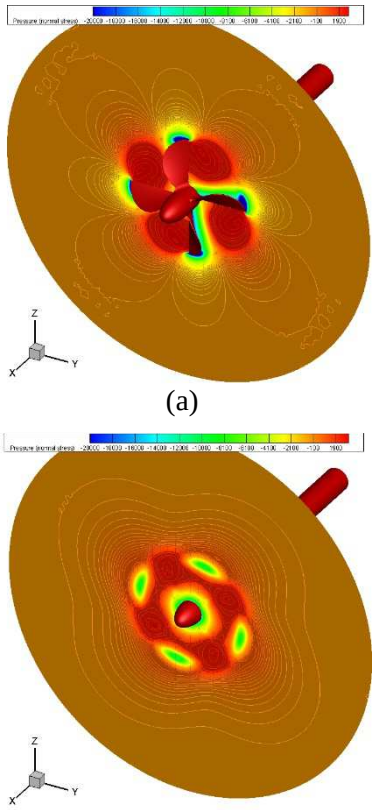

(a)

(b)

Fig. 6. Pressure (normal stress) distributions in: (a) - the propeller plane and (b) – at 0.1 D_P downstream of the propeller plane

The attenuation in the radial direction is also significant, a fact that may suggest that the rotational effect induced by the propeller manifests inside of a tube of fluid which is restricted, more or less, to the propeller diameter. Inside of that tube there is a strong vortical flow characterize by periodic pressure and velocity pulses equally spaced and having a periodicity directly related to the rate of rotation of the propeller. Physically they act as hydrodynamic rollers in which a vortex is replaced by a new generated one and washed down in the steam until eventually vanishes because of the viscous interactions. The cores of the vertices are of a lower energy that the surrounding fluid so the dissipation is not only helped, but somehow accelerated. Obviously, this mechanism is well reproduced in Fig. 7, which bears out the distribution of the pressure in two perpendicular planes, i.e. x=0 and y=0.

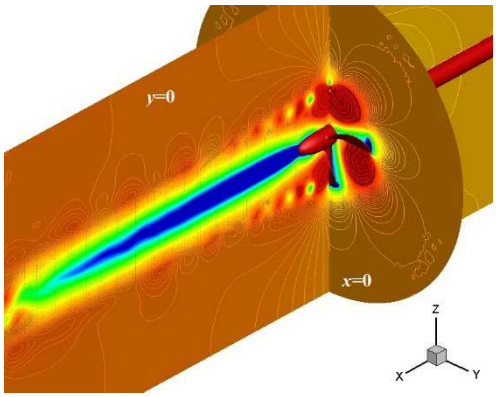

Fig. 7. 3D pressure field distribution in the propeller plane and in the longitudinal plane of symmetry.

The pressure pulses are closely related to the other main hydrodynamic parameters such as the axial velocity component or the turbulent kinetic energy since they are linked by the PDE set of equations that is numerically solved. Figure 8(a), which depicts the axial velocity field as well as Fig. 8(b) that show the turbulent kinetic energy field in the propeller wake may prove the statement

© Galati University Press, 2017

made in the paragraph above. Worth mentioning that there is no phase shift between the cores of the vortices, a fact that may suggest the physical consistency of the solution. The vortical structure of the flow has an important influence not only of the propeller itself, but also on the rudder efficiency since the control surface of the governing system is working in the propeller wake. That is, the fluctuating velocity and pressure fields in the wake of the propeller will determine fluctuations in the lift force and moment at the rudder shaft. At least from this point of view a deeper insight into the mechanism of their production and development is desired.

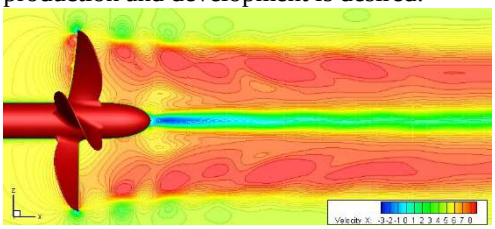

(a)

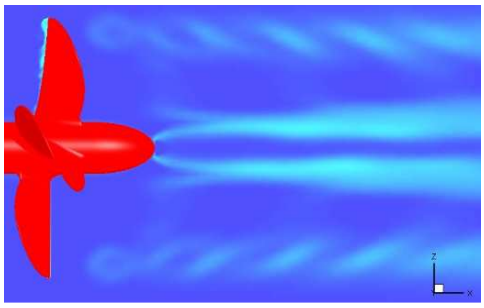

(b)

Fig. 8. Axial velocity (a) and turbulent kinetic energy (b) distributions in the vertical symmetry plane of the domain

A general overview of the vortical behavior of the flow developed in the wake of the propeller is proposed in Fig. 9, which depicts the iso-surfaces of the second invariant colored by helicity for two different loading conditions, namely J=0.25 and J=0.75. The theory states that regardless of the advance ratio, the trajectory of tip vortex in the longitudinal plane is expected to incline towards the hub, a fact that may suggest a contraction of the trajectories of the tip vortices, as Fig. 7 and Fig. 8(a) show. This behavior is more significant when the advance ratio decreases, as Fig. 9 proves. Three vortical entities are detected in the wake of the propeller. The main one is released by propeller tips and is the strongest in intensity. The second one is associated to the roots, it is weaker and of a larger period when the rotational velocity is small or moderate. Finally, there is a third one produced by the hub, which acts as a filament.

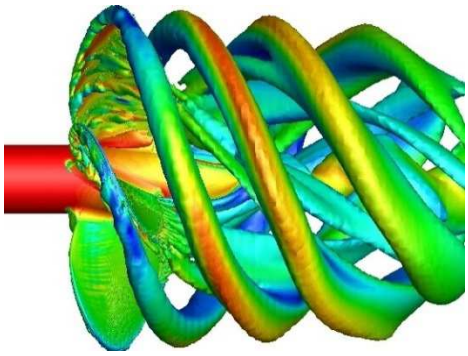

(a)

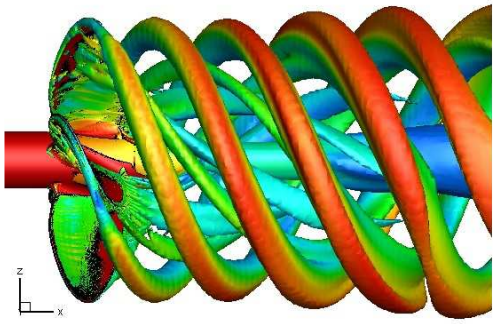

(b)

Fig. 9. Isosurfaces of the second invariant of velocity computed at J=0.25 and J=0.75 and colored by helicity

The intensity of the vortices is getting weaker far in the propeller wake, a fact which is due to the viscous interaction with the rest of the fluid. As a result, the vortical structures either vanish or collapse into each other. When the downstream distance increases, the propeller wake restores to the

© *Galati University Press, 2017*

free-stream flow gradually and the fluctuation of the circumferential distribution of axial velocities becomes also weaker.

4. NUMERICAL SIMULATION OF THE CAVITATION

Generally speaking, cavitation is defined as a rapid decrease of pressure resulting in a phase change from an initially homogeneous liquid to vapor. Usually, cavitation occurs when the liquid is highly accelerated and the vapor bubbles produced by the pressure drop induces adverse effects such as thrust and efficiency reductions. The phenomenon is strongly non-linear, develops violently in time and space, therefore it requires a special attention for the discretization.

A very fine mesh in all the areas where cavitation is expected to appear is a must, although it does not automatically guaranty a valid result. That supposes an initial pilot computation for detecting all those susceptible areas. The unsteady approach is chosen for the numerical simulation. When switching to the cavitation, although a time discretization of first order is considered as being sufficient, in the present study a second order has been the choice despite the costs in terms of the CPU and the memory usage. The time step is chosen to fulfill the following condition:

$$\Delta t = \frac{C_{0.7R}}{100\sqrt{U_\infty^2 + (2\pi n \cdot 0.7R)^2}}$$

where $C_{0.7R}$ is the blade chord at 70% of radius, U_∞ is the advance speed of the propeller, n is the rotational speed of the propeller expressed in rad/s and R is the radius of the propeller.

In mono-fluid computations the boundary condition at the downstream is set at a prescribed pressure, namely the frozen pressure, whose value is 0 in a mono-fluid computation. In a multi-fluid computation the free-surface (which means the variable surface between the vapor and water species) the 0 pressure is used as reference pressure. The vapor pressure is set relatively to this reference pressure, so the vapor pressure value will be negative. For our particular case, the vapor pressure of water at 15 degrees is 1700 Pa, therefore the reference is not atmospheric pressure but 0, so the vapor pressure is P_v-P_{atm} = -99 625 Pa. The other input key parameters for the cavitation simulation are p_{gain}=1·10^5 for the pressure gain, 1000 pressure iterations, while the third level is chosen for the incomplete LU factorization as a preconditioner in this case. Although the previous computations for the open water propeller have proven that the EASM model performed better, in this particular case the $k-\varepsilon$ model is employed by default to solve the turbulence-related issues in the present simulation.

All those being said, in the followings a brief insight of the mathematical model used for the cavitation simulation will be given. ISIS-CFD treats the cavitation as being based on the resolution of a transport equation similarly to what is done for free surface, although the significance of the free-surface is completely different to that which concerns the water waves. In this particular case the source terms used in modeling the vaporization and condensation of the two phases.

Let C_i be the volume fraction used to compute the evolution of the free surface, therefore $\alpha_a = 1 - C_i$ gives the volume fraction of air. Let then C_iC_{av} be a variable that defines the vapor fraction or the liquid fraction. Supposing that α_a, α_v and α_l are the volume fractions of air, vapor and liquid, the following equation is straightforward:

$$\alpha_a\rho_a + \alpha_v\rho_v + \alpha_l\rho_l = \rho$$

and the equation of mass conservation ultimately becomes as follows:

$$\frac{\partial\rho}{\partial t} + div(\rho\vec{U}) = \rho_a\left(\frac{\partial\alpha_a}{\partial t} + div(\alpha_a\vec{U})\right) + \rho_v\left(\frac{\partial\alpha_v}{\partial t} + div(\alpha_v\vec{U})\right) + \rho_a\left(\frac{\partial\alpha_l}{\partial t} + div(\alpha_l\vec{U})\right)$$

© Galati University Press, 2017

If $(1 - C_i C_{av})$ represents the vapor fraction α_v _v, then $C_i = \alpha_l + 1 - C_i C_{av}$ represents the volume fraction of both liquid and vapor. The volume fraction of liquid is given by the equation:

$$\alpha_l = C_i + C_{av} - 1$$

it results in:

$$div(\vec{U}) = -\left(\frac{\rho_l - \rho_v}{\rho_v}\right)\dot{m}_l = \left(\frac{\rho_l - \rho_v}{\rho_l}\right)\dot{m}_v$$

or in:

$$\dot{m}_v = -\frac{\rho_l}{\rho_v}\dot{m}_l$$

where $\dot{m}_l$ and $\dot{m}_v$ represent the vaporization of the liquid and the condensation of the vapor, whereas ρ_l and ρ_v are the densities for the liquid and vapor, respectively. With all these particular specifications the Kunz model finally reads as follows [5], [6]:

$$\frac{\partial \alpha_l}{\partial t} + div(\alpha_l \vec{U}) = \dot{m}_l = \frac{C_{dest}^{liq}}{(0.5\rho_l U_\infty^2)T_\infty}\frac{\rho_v}{\rho_l} Min(P - P_v, 0)(\alpha_l) + \frac{C_{prod}^{liq}}{T_\infty}\frac{\rho_v}{\rho_l}(\alpha_l)^2(1 - \alpha_l)$$

$$\frac{\partial \alpha_v}{\partial t} + div(\alpha_v \vec{U}) = \dot{m}_v = \frac{C_{prod}^{vap}}{(0.5\rho_l U_\infty^2)T_\infty} Min(P - P_v, 0)(\alpha_l - 1) + \frac{C_{dest}^{vap}}{T_\infty}\frac{\rho_v}{\rho_l}(1 - \alpha_v)^2\alpha_v$$

Based on the study of Morgut et al. [7], the default values for the parameter coefficients are 4100 for the liquid destruction term and 455 for the liquid production term.

Fig. 10 depicts the evolution of the cavitation sheet at three different time steps, namely T1=2.5s, T2=5s and T=7.5s after the cavitation model was set. Sheet cavitation is the region of vapor which remains approximately at the same position relative to the propeller blade, appearing as being attached to the foil. Obviously, although the simulation could capture the development of the cavitation sheet, more studies are required in the future for clarifying the intrinsic details of the phenomenon.

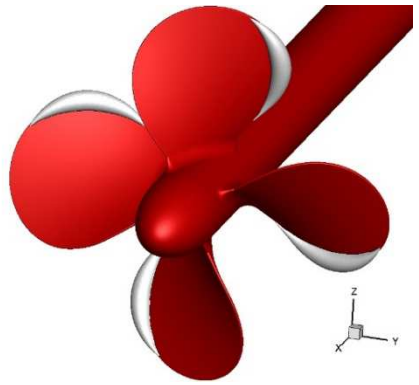

(a)

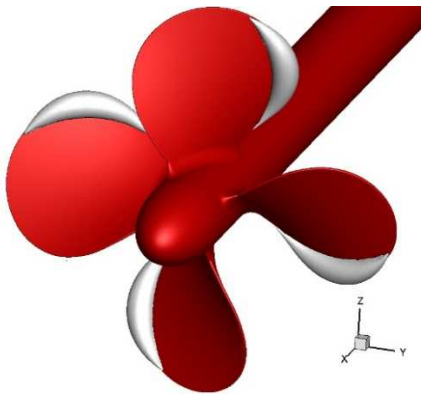

(b)

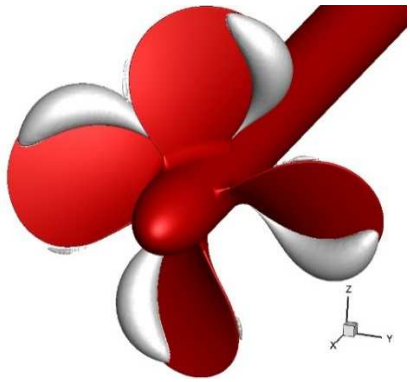

(c)

Fig. 10. Evolution of the cavitation sheet

© *Galati University Press, 2017*

5. CONCLUDING REMARKS

The 3D unsteady flow around the ONRT propeller is numerically simulated to establish the computed hydrodynamic performances through comparisons with the experimental data existing in the public domain [1]. The simulation is accomplished in a global approach in which the solution for the RANS equations written in respect to a Cartesian system of coordinates is advanced in time in a classical Euler manner.

Although not described in the present paper, a detailed grid convergence test was performed on three different grids on which the solution was computed. A detailed analysis of the local flow features was also performed and several qualitative conclusions were withdrawn.

The comparisons between the numerical solution of the simulation and the experimental data proved that the ISIS-CFD flow solver may reproduce with a satisfactory accuracy the hydrodynamic behavior of propeller working in open water.

Acknowledgements

The research was supported by the Research Centre of the Naval Architecture Faculty, in "Dunarea de Jos" University of Galati, which is greatly acknowledged.

REFERENCES

[1]. **NMRI** (2015), *"Tokyo 2015 A Workshop on CFD in Ship Hydrodynamics"*, retrieved from http://www.t2015.nmri.go.jp/

[2]. **Sanada, Y., Tanimoto, K., Takagi K, et al.,** *"Trajectories for ONR Tumblehome Maneuvering in Calm Water and Waves"*, Ocean Engineering, 72, pp. 45–65, 2013.

[3]. **Rumsey, C.L., Gatski, T.B.,** *"Recent Turbulence Model Advances Applied to Multielement Airfoil Computations"*, Journal of Aircraft, Vol. 38, No.5, pp. 904–910, 2001.

[4]. **Duvigneau, R., Visonneau M. Deng, G.B.,** *"On the Role Played by Turbulence Closures in Hull Ship Optimization at Model and Full Scale"*, Journal of Marine Science and Technology, 8, pp. 11–25, 2003.

[5]. **Merkle, C.L., Feng, J., Buelow, P.E.O.,** *"Computational modeling of the dynamics of sheet cavitation"*, 3rd International Symposium on Cavitation, Grenoble, France, 1998.

[6]. **Kunz, R.F., Boger, D.A., Stinebring, D.R., Chyczewski, T.S., Lindau, J.W., Gibeling, H.J., Venkateswaran, S. T.R.Govindan,** *"A preconditioned Navier–Stokes method for two-phase flows with application to cavitation prediction"*, Computer and Fluids, Volume 29, Issue 8, pp. 849-875, 2000.

[7]. **Morgut, M., Nobile, E., Bilus, I.,** *"Comparison of mass transfer models for the numerical prediction of sheet cavitation around a hydrofoil"*, International Journal of Multiphase Flow, 2011.

Paper received on September 15th, 2017

 © Galati University Press, 2017